Lithium ion micrometer diffusion in a garnet-type cubic $Li_7La_3Zr_2O_{12}$ (LLZO) studied using ^7Li NMR spectroscopy

Kikuko Hayamizu, Shiro Seki, and Tomoyuki Haishi

Citation: J. Chem. Phys. **146**, 024701 (2017); doi: 10.1063/1.4973827
View online: http://dx.doi.org/10.1063/1.4973827
View Table of Contents: http://aip.scitation.org/toc/jcp/146/2
Published by the American Institute of Physics

RIGHTSLINK

Lithium ion micrometer diffusion in a garnet-type cubic $Li_7La_3Zr_2O_{12}$ (LLZO) studied using ^7Li NMR spectroscopy

Kikuko Hayamizu,[1,a)] Shiro Seki,[2] and Tomoyuki Haishi[3]
[1]*Institute of Applied Physics, University of Tsukuba, Tennodai, Tsukuba 305-8573, Japan*
[2]*Material Science Laboratory, Central Research Institute of Electric Power Industry, Nagasaka, Yokosuka 240-0196, Japan*
[3]*MR Technology, Inc., Sengen, Tsukuba 300-0047, Japan*

(Received 15 September 2016; accepted 27 December 2016; published online 13 January 2017)

Mobile lithium ions in a cubic garnet $Li_7La_3Zr_2O_{12}$ (Al-stabilized) were studied using ^7Li NMR spectroscopy for membrane and powder samples, the latter of which was ground from the membrane. Lithium diffusion in a micrometer space was measured using the pulsed-gradient spin-echo ^7Li NMR method between 70 and 130 °C. When the observation time (Δ) was shorter than 20 ms, the echo attenuation showed diffusive diffraction patterns, indicating that the Li^+ diffusing space is not free but restricted. For longer Δ, the values of apparent diffusion constant ($D_{apparent}$) became gradually smaller to approach an equilibrated value (close to a tracer diffusion constant). In addition, the $D_{apparent}$ depends on the pulse field gradient strength (g) and became smaller as g became larger. These experimental results suggest that the lithium ions diffuse through Li^+ pathways surrounded by stationary anions and lithium ions, and are affected by collisions and diffractions. One-dimensional profiles of the membrane sample of thickness 0.5 mm were observed from 65 to 110 °C and the area intensity, as well as the lithium occurrence near the surface, increased with the increase in temperature. The temperature-dependent area intensity showed a correspondence to the number of Li^+ carrier ions estimated from the ionic conductivity and the equilibrated diffusion constant through the Nernst-Einstein relationship. *Published by AIP Publishing.* [http://dx.doi.org/10.1063/1.4973827]

I. INTRODUCTION

A garnet-type conductor $Li_7La_3Zr_2O_{12}$ (LLZO) and related materials have attracted much attention because of their large ionic conductivity and possible safe application to all-solid lithium ion batteries. Recent studies of garnet-type conductors for lithium batteries have been reviewed by Thangadurai *et al.*[1] From the discovery of fast ion conduction in a garnet-type LLZO,[2] extensive studies on synthesis and structure analysis using X-ray analysis and conductivity measurements have been performed and indicate the existence of two crystalline structures, i.e., cubic and tetragonal crystalline structures.[3–5] It was noticed that the synthesized LLZO included a small amount of Al from an Al-crucible. In addition, under open circumstances, H_2O easily reacts with Li and the exchange occurs between proton and Li^+. The formed LiOH reacts with atmospheric CO_2 to form Li_2CO_3. The structure is unstable.[6–9] Then, CO_2-doped LLZO was prepared,[6] and the structural stability was shown to be related with hydration studied by X-ray analysis[7–9] and ^6Li NMR related with ^1H coupling.[9] The addition of metals such as Al, Ga, Sr, Zr, Nb, Sb, Te, Ba, Ta, and others was attempted to increase the structural stability and ionic conductivity.[10–23] The synthesis of new conductors, of which structures are always studied by X-ray analysis, and their fast ionic conduction are most important subjects.[12–15,17,18] Furthermore, magic-angle sample-spinning (MAS) solid-state NMR spectra of ^{27}Al, ^6Li, and ^7Li have been observed to study the structures and Li mobility.[10,11,15] Nanowires and particles were used to synthesize cubic and tetragonal LLZO.[24] The synthetic procedure was monitored using *in situ* neutron diffraction to find out rational processes for garnet electrolytes.[25]

The phase transformations between the tetragonal and cubic phases of LLZO have been studied. The tetragonal phase is stable owing to the crystalline structure and the cubic phase transition occurs above 700 °C. The ionic conductivity of cubic-LLZO is higher than that of tetragonal-LLZO at room temperature. In this situation, origin of the phase transition and the mechanisms of lithium ion conduction have been studied.[26–29] In addition to the high-temperature phase transition, the tetragonal crystal was shown to have a phase transformation at low temperature (LT) between 100 and 150 °C to form a LT cubic phase studied by X-ray diffraction (XRD) observation.[23,30–32]

Lithium conduction pathways and lithium distribution in the LLZO have been reported using neutron diffraction, and the Li^+ transport was proposed through short-range pathways in nm order.[33,34] Computational methods have been applied to understand lithium local structure and dynamics.[27,35–38] Estimation for the number of mobile lithium ions was proposed for garnet-type solid conductors.[22,39,40]

The important focus on these materials has been high ionic conductivity, which originates from lithium ion migration. Although direct measurements of the lithium position cannot be obtained by the XRD method, neutron diffraction can

a)Author to whom correspondence should be addressed. Electronic mail: hayamizu.k3@gmail.com

RIGHTSLINK

provide information on lithium ion distribution. Magic-angle sample-spinning solid-state NMR methods have been applied to study the structures of LLZO and related conductors using ^{6}Li, ^{7}Li, ^{27}Al, and ^{71}Ga resonances.[9–11,14,15,38,41,42] Steady-state ^{7}Li spectra without motional narrowing are broad and affected by quadrupolar couplings (nuclear spin I of ^{7}Li = 3/2).[42–45] The motional narrowing of the ^{7}Li spectral lines takes place with an increase in temperature by lithium ion vibration and jumps. The local mobility of lithium ions can be observed by the ^{7}Li relaxation times, which are assumed to be related with fast ion conduction and observed in wide ranges of temperature and frequency, and precise analysis has been developed about the fast lithium jump.[42–47] The ^{7}Li relaxation is mainly influenced by one or several jumps of lithium ions in a time scale of 10^{-4} (below room temperature) to 10^{-9} s in 10^{-10} m space. These studies have been devoted to understand atomic-scale details.

Since solid-conductors are used mainly in micrometer or larger sizes for electrochemical devices, information is required for lithium migration on longer scales, including grain boundaries. The pulsed-gradient spin-echo (PGSE) ^{7}Li-NMR method can provide migration in μm space. Up to now, we have measured self-diffusion constants of lithium ion, anions, and solvents in various solution electrolytes, in which the electrolyte systems are homogeneous and not required to introduce the concept of diffusion distance,[48–50] except for polymer electrolytes.[51,52] The lithium ion migration circumstances in solid conductors are complicated in μm space and not a simple extension of the ion migration in atomic-scale space or homogeneous circumstances.

We have measured lithium migration in a garnet-type LLZO-Ta[53] and sulfide-type solid conductors[54–56] using the PGSE NMR method and found that the lithium migration depends on observation time Δ and pulse-field gradient (PFG) strength g. These phenomena suggest that the lithium ion migration in μm space is distributed heterogeneously and polydispersively in the solid conductors.

In our previous studies, lithium ion diffusive diffractions were observed for short Δ, in which lithium ions migrate very quickly. Diffusive diffraction patterns for short Δ were insensitive to temperature throughout the range studied. Generally, the diffusive diffraction phenomena have been studied by the PGSE-NMR method under the concept of restricted diffusion for molecules confined in various types of space and analyzed by experimental and theoretical approaches.[57–62] When the diffractive patterns are observed, the echo attenuations are plotted in q-space ($q = \gamma\delta g/2\pi$) and the inverse of the first diffraction minimum is related to the radius of the restricted space. The systems hitherto developed have been concentrated to neutral fluid molecules such as H_2O diffusing in neutral circumstances such as polymers, glasses, and so on.[57–62] The significance was suggested for the fluid-surface interaction in the q-space data.[60] Generally, mass transfer in mesoporous materials was reviewed by Kärger and Valiullin.[63]

In this study conduction is carried by Li^+ ions and migrating ^{7}Li species are charged positive and stationary $La_3Zr_2O_{12}$ must be charged negative. For the fast $^{7}Li^+$ migration in the solid, the long-range lithium pathways are formed through walls charged negative. The distribution of negative charge on the wall of $La_3Zr_2O_{12}$ has not yet precisely studied. The diffractive patterns in short Δ clearly suggest that the Li^+ ions do not diffuse in free space and must be affected by the coulomb interaction. The ^{7}Li diffusive diffraction patterns in solid conductors[53–56] showed quite unexpected behaviors from the well-established restricted diffusion models. To analogy to the restricted diffusion, the echo attenuations were plotted in the q-space and diffraction minimum is assumed to give the distance until collision.[61,62] The analysis will give important information on structures of the walls and long-range lithium pathways. The mobile lithium ions diffuse accompanied by repeated collisions to stationary walls and diffractions. The diffraction manners were scattered over several μm, depending on the observation time, Δ, and the PFG strength, g, and also internal structures in μm space of solid conductors. In some meanings, the diffractive patterns are snapshots for migrating lithium ions.

In this study, we observed the ^{7}Li NMR spectra and lithium ion migration behaviors of cubic LLZO between room temperature and 140 °C for membrane and powder samples to compare the sample size effects. The ^{7}Li spectra of both samples obtained by steady-mode NMR were composed of narrow and broad components. The linewidth of the narrow component became sharper with increasing temperature, allowing diffusion measurements possible above 70 °C using the PGSE NMR method. The target of the diffusion measurements was limited to the narrow component. At 140 °C the broad component was observed in both the samples and this fact is different from our previous studies in solid conductors, in which the broad component disappeared at a high temperature in cubic LLZO-Ta,[53] and an amorphous sulfite solid conductor.[54–56] Lithium diffusion was observed by changing Δ and g.

We also measured the Δ dependent apparent diffusion constant ($D_{apparent}$) to approach an equilibrium value (close to tracer diffusion constant) to compare the ionic conductivity.

Since the membrane sample can provide a good disk shaped with a thickness of 0.5 mm and a diameter of 3 mm, one-dimensional ^{7}Li profiles in the thickness direction were observed with increasing temperature. The area intensity increased with temperature and related with the number of charge carrier lithium ions estimated from the ionic conductivity and the tracer diffusion constant through the Nernst-Einstein relationship.

The ^{7}Li NMR diffusion measurement results were complicated and we tried to confirm our experimental results for different types of solid conductors. About one year after the sample preparation, we remeasured the LLZO samples which were kept in flame-sealed NMR tubes at ambient temperature. The results were almost reproducible within experimental errors, and we found that the diffraction patterns were reduced and the linewidth of the broad component decreased. We assume that slow structure relaxation exists in μm space for the present solid conductors.

II. EXPERIMENTAL DETAILS

A. Sample preparation

The membrane sample of cubic LLZO (Al-stabilized one) was purchased from TOSHIMA Manufacturing, Co., Ltd

RIGHTSLINK

(Saitama, Japan). The structure was confirmed as a pure cubic crystal using the powder XRD pattern. The thickness of the membrane was controlled to be 0.5 mm. The powder sample was prepared by grinding the membrane by hand in an Ar-filled glove box. The membrane and powder samples were inserted in an NMR sample tube equipped with an inner glass tube, BMS-005J (Shigemi, Tokyo, Japan) with a height of 5 mm in the grove box and flame sealed. The LLZO sample was confined in a small space and exposure to Ar gas was minimized. A disk sample with a diameter of 3 mm was prepared by punching the membrane sample and placed in the NMR tube horizontally and flame sealed to observe one-dimensional ^{7}Li profiles in the direction of the thickness.

B. Ionic conductivity measurement

AC impedance measurements were performed on a dense pellet using platinum layers sputtered on both sides of the membrane, and Pt meshes and wires were attached to current collectors. The ionic conductivity (σ) was measured on [stainless steel (SUS)/electrolyte sample/SUS] hermetically sealed cells and determined using the complex impedance method with an AC impedance analyzer (VSP, Bio-Logic, 200 kHz–50 MHz; applied voltage: 10 mV) between 373 and 333 K at 5 K intervals while cooling the samples. The samples were thermally equilibrated at each temperature for at least 90 min prior to measurement.

C. Scanning electron microscopy (SEM) measurements

Scanning electron microscopy (SEM; JCM6000, JEOL, Tokyo, Japan) was used to characterize the surface morphology of the LLZO pellet and powder samples.

D. NMR measurements

The ^{7}Li NMR spectra were measured on a Tecmag Apollo spectrometer (Houston, TX, USA) equipped with a 4.7 T wide-bore magnet using a PFG probe (JEOL). Generation of a well-shaped rectangular PFG is possible using a JEOL probe and amplifier (50 A) as shown in Fig. S11 of the supplementary material. The precise calibration of PFG strength g and duration time δ was performed using D_2O and an ionic liquid, 1-ethyl-3-methylimidazolium bis(trifluoromethylsulfonyl)amide (EmimTFSA)[64] as shown Fig. S13 of the supplementary material. In Figs. S12 and S14 of the supplementary material, the ^{1}H signals of EmimTFSA are shown to remain in the same positions without and with PFG application. We can assume negligible background DC current and monopolar pulse sequences can provide accurate experimental results. The ^{7}Li NMR spectra were measured at 78.4 MHz. Lithium diffusion was observed by the stimulated echo (STE) PGSE-pulse sequence shown in Fig. 1(a). One-dimensional ^{7}Li profiles were observed using the pulse sequence in Fig. 1(b).

Since the aim of this study is the observation of Li^+ migration in a μm space, all of the measurements were performed between 30 and 140 °C by a steady mode with 90° pulse of approximately 10 μs. Since the values of ^{7}Li T_1 and T_2 are necessary to set the measurement parameters, the determination

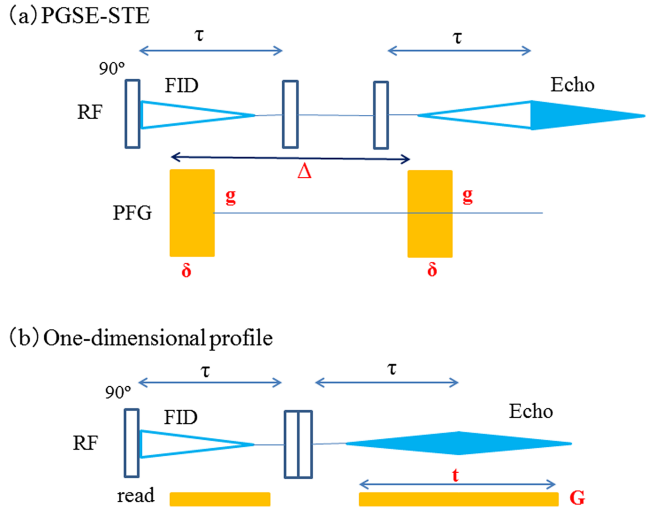

FIG. 1. The pulse sequences of (a) STE-PGSE in which two PFGs of strength g and duration time δ are applied with the time interval Δ and (b) one-dimensional profile with read gradient fields of height G and t during whole echo acquisition and $t/2$ during FID after the first 90° pulse.

of T_1 and T_2 was performed by the pulse sequences of 180°-τ-90°-acquisition (FID signal) and 90°-τ-180°-τ-acquisition (half echo signal), respectively. In the PGSE experiments, the first PFG marks the initial position to encode lithium ions and the second PFG detects the position of migration for the encoded lithium ions after Δ. The echo attenuation does not include any information on the procedure during Δ.

The echo attenuation E is related to the experimental variables (g, δ, and Δ), and the diffusion coefficient, D, can be obtained using the Stejskal and Tanner equation for a homogeneous space,[65,66]

$$S(g,\delta,\Delta) = \frac{E}{E_0} = \exp(-\gamma^2\delta^2 g^2 D(\Delta - \delta/3)) = \exp(-bD), \tag{1}$$

where γ is the ^{7}Li gyromagnetic ratio ($1.039\,77 \times 10^{8}$ s^{-1} T^{-1}). In general, the echo attenuation can be observed on either a fixed g value by varying δ or with a fixed δ value by varying g. In homogeneous systems, both measurements provide the same D value, which is independent of g and Δ, but this is not always true in LLZO-Ta.[53] A single-exponential diffusion plot using Eq. (1) shows the free diffusion of a single diffusion species. In this study, g was set to a value between 4.8 and 13 T m^{-1}. For a fixed value of g, δ was varied between 0.2 and 4 ms (16 increments) with τ = 4.4 ms. Since ^{7}Li T_2 of solid conductors are generally very short, we confirmed the validity of the PGSE NMR measurements for samples having short T_2 values. As an example, testing procedures of diffusion plots are shown in Fig. S15 of the supplementary material for a sulfide-type solid conductor (T_2 = 2.8 ms at 25 °C). In the pulse sequence in Fig. 1(a), Δ, g, and δ are maintained in the same conditions and the τ value was changed from 4.2 to 6.8 ms to observe the echo attenuations. Although the sensitivity was influenced significantly by the τ values, the plotted patterns and the D_{apparent} values were almost unchanged. In this situation, we did not recognize eddy current effects. The echo signals were averaged between 32 and 256 times depending on the measurement conditions.

RIGHTSLINK

The one-dimensional ^{7}Li profile was measured by the pulse sequence shown in Fig. 1(b), in which the amplitude G of the read gradient field was 3.4 T m^{-1}, and t = 2.56 ms. The corresponding pixel was 7 μm (like spatial resolution) calculated by $k = \gamma t G/2\pi$ [m^{-1}]. The profile scale agreed well with the actual membrane size.

III. RESULTS AND DISCUSSION

A. SEM and ionic conductivity

SEM images of the membrane and powder samples are shown in Fig. S1 of the supplementary material. Clearly, grinding effects are shown in the images of the powder sample. An Arrhenius plot of the ionic conductivity is shown in Fig. S2 of the supplementary material for the membrane sample. The activation energy was about 71 kJ mol^{-1}.

B. ^{7}Li spectral pattern

^{7}Li spectra of the membrane and powder samples were observed from room temperature to 120 °C. An example is shown in Fig. S3 of the supplementary material for the membrane sample at 80 °C and indicates that narrow and broad components coexist. Because lithium ions in rigid states are known to show very broad lines,[42,43] motional narrowing processes exist in the present temperature range. Each spectrum was fitted by an overlap of two Lorentz-type curves using Origin 9.0 software. The temperature dependences of the line widths of narrow and broad components obtained by fitting the spectral patterns of two Lorentz-type curves are shown in Fig. S4 of the supplementary material for the membrane and powder samples.

In general, the line width was smaller in the membrane sample than in the powder sample, especially in the low temperature region. The sample forms and sizes of the solid conductors affect the ^{7}Li spectral patterns. Although the temperature dependence of the line width for the narrow component was small (0.4 to 0.3 kHz for the powder sample and slightly sharper for the membrane sample), the broad component showed a large temperature dependence (8 to 2 kHz). The narrow component may include a quadrupolar −1/2 to 1/2 transition of the broad component. Actually, the line width of echo signals of PGSE measurements became slightly smaller than that of the corresponding narrow component. The ratio of area intensity of the narrow component increased slightly with the increase in temperature and the narrow component was about 60% in both the membrane and powder samples at 120 °C. The ^{7}Li echo signals do not include a broad component in the cubic LLZO samples. We kept the samples at an ambient temperature sealed in a NMR sample tube. After one year, we found that although the T_1 and T_2 values and the line width of the narrow component remained unchanged, the line width of the broad component became slightly smaller at 120 °C than that for the samples just after preparation, suggesting slow structure relaxation in less mobile lithium ions.

C. ^{7}Li T_1 and T_2

The observation of T_1 and T_2 of the narrow component was performed for the membrane and powder samples, as shown in Fig. S5 of the supplementary material. The decay curves for the relaxation measurements (both T_1 and T_2) were analyzed by a single-component exponential decay. The data of T_1 and T_2 for the membrane and powder samples agreed within experimental errors. Almost the same activation energies of T_1 were obtained as 10.2 ± 0.1 and 10.6 ± 0.1 kJ mol^{-1} for the membrane and powder samples, respectively. The sample size was insensitive to the ^{7}Li T_1 and T_2. As the temperature increased, T_2 became longer from 0.7 to 4 ms, and longer T_2 was better for the sensitivity of the PGSE NMR. Conversely, T_1 became shorter with the increase of temperature from 0.15 to 0.06 s, and longer accumulation of the echo signals was required for the long Δ measurements. The PGSE NMR could be performed above 65 °C (T_2 > 2 ms).

D. Δ-dependent diffusion

As shown previously for LLZO-Ta[53] and sulfide-type lithium conductors,[54–56] the diffusion plot following Eq. (1) was dependent on g and Δ. As examples, Δ-dependent diffusion plots of the powder sample at 70 °C and of the membrane sample at 120 °C are shown in Figs. 2 and 3, respectively.

Clearly, Δ-dependent diffusion plots were observed for both the membrane and powder samples. The diffusive diffraction plots were observed for Δ = 10 and 20 ms. From the initial linear decay of the echo attenuation, the $D_{apparent}$ was estimated using Eq. (1). As described later, the diffractive patterns at Δ = 20 ms disappeared after one year.

The Δ-dependence of the $D_{apparent}$ value was plotted in Fig. 4 for the membrane and powder samples obtained at 70 and 120 °C between Δ = 20 and 70 ms. The small difference in values of the $D_{apparent}$ for short Δ is noticeable. As Δ became longer, the values of $D_{apparent}$ became smaller and scattered in each observation. The value of $D_{apparent}$ approached an equilibrium value for Δ = 70 ms.

Clearly, as Δ became longer, the values of $D_{apparent}$ became explicitly smaller. From Δ = 20 to 70 ms, the lithium diffusion values were reduced to less than approximately 10%. To

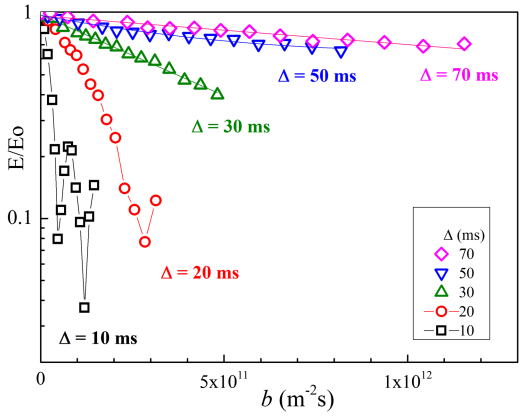

FIG. 2. Δ-dependent diffusion plots of the powder sample at 70 °C under a fixed g = 9.8 T m^{-1} and δ was varied from 0.2 to 4 ms (16 increments). The initial decay of Δ = 10 (square) and 20 ms (circle) gave $D_{apparent}$ = 31 and 5.9 × 10^{-12} m^2 s^{-1}, respectively. The echo attenuations at Δ = 30 (up-triangle), 50 (down-triangle), and 70 ms (diamond) could be fitted to give $D_{apparent}$ values of 18, 3.6, and 3.1 × 10^{-13} m^2 s^{-1}, respectively. The $D_{apparent}$ value was 3.0 × 10^{-13} m^2 s^{-1} at 200 ms (not shown).

RIGHTSLINK

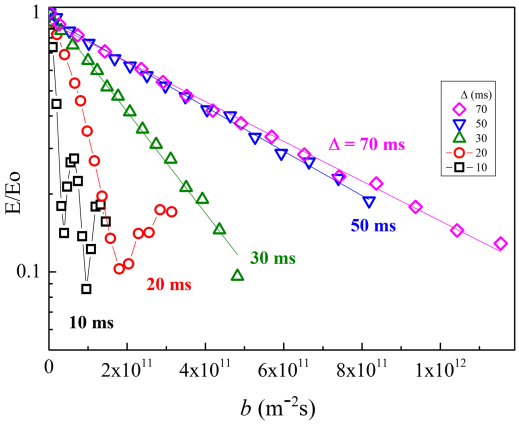

FIG. 3. The diffusion plots of the membrane sample at 120 °C for Δ = 10 (square), 20 (circle), 30 (up-triangle), 50 (down-triangle), and 70 ms (diamond) in which g was fixed at 9.8 T m^{-1} and δ was varied from 0.2 to 4 ms (16 increments). The $D_{apparent}$ values were 31, 11, 4.3, 1.9, and 1.6 × 10^{-12} m^2 s^{-1}, for Δ = 10, 20, 30, 50, and 70 ms, respectively. The scattering behaviors depending on Δ are a kind of snapshots.

our knowledge, these phenomena are observed for lithium ion diffusion in solid conductors.

E. *g*-dependence

Previously, we have reported g-dependent lithium diffusion in LLZO-Ta[53] and sulfide solid conductors.[54–56] In this work, the g-dependent diffusion was observed with a fixed g varying δ measurements and confirmed with Δ = 50 ms at 120 °C for both samples. The diffusion plots were almost linear with Δ = 50 ms, as shown in Fig. 5.

Clearly, the $D_{apparent}$ value became smaller as g became larger. Generally, quickly diffusing species in liquids can be observed using a small g, and when the diffusion is slower, larger g is required to obtain enough decays of the echo attenuation for a smaller diffusion constant. The $D_{apparent}$ values obtained at g = 12.4 T m^{-1} and Δ = 50 ms are close to the values obtained at g = 9.8 T m^{-1} and Δ = 70 ms. In this work, similar to our previous papers concerning LLZO-Ta and sulfide solid conductors, clear g-dependent diffusion was observed in both the powder and membrane samples at high

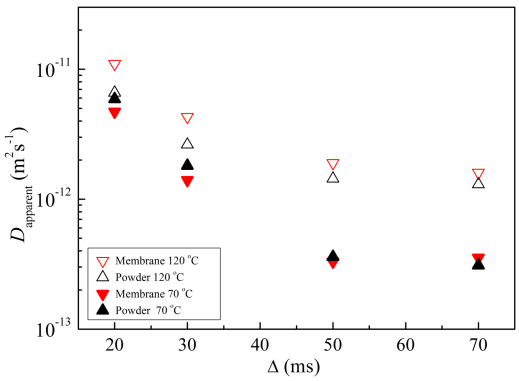

FIG. 4. $D_{apparent}$ plotted versus Δ for the membrane (down-triangle) and powder (up-triangle) samples at 120 °C (open) and 70 °C (solid). For Δ = 20 ms, the diffraction patterns were observed for the four measurements and the $D_{apparent}$ values were estimated from the initial linear decays. When Δ was longer, the diffusion plots were almost linear in the whole range measured.

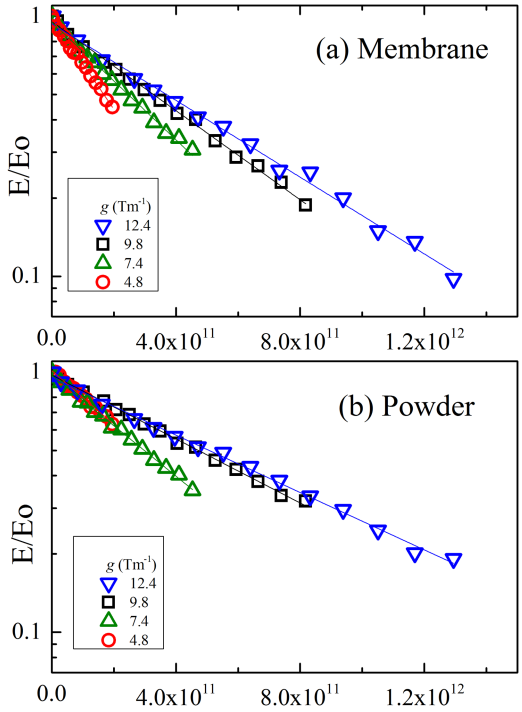

FIG. 5. g-dependent diffusion plots of (a) membrane and (b) powder samples observed at 120 °C with a fixed Δ = 50 ms from g = 4.8 to 12.4 T m^{-1}, in which δ was varied from 0.2 to 4 ms (16 increments). The $D_{apparent}$ values were 4.0, 2.6, 2.0, and 1.7 × 10^{-12} m^2 s^{-1} (membrane sample) and 2.4, 2.2, 1.4, and 1.3 × 10^{-12} m^2 s^{-1} (powder sample) for g = 4.8, 7.3, 9.8, and 12.4 T m^{-1}, respectively.

temperature. Similar g-dependent diffusion was observed also at lower temperatures and shorter Δ. The phenomenon of g-dependence may be interpreted in terms of an inhomogeneous system in which lithium ions diffuse in heterogeneous and polydispersive manners. Within the same time interval, lithium ions move in scattered diffusion constants and we cannot specify a unique value of diffusion coefficient at a certain temperature. When the diffusion measurements are performed with a fixed value of δ varying g in Eq. (1), the value of $D_{apparent}$ became larger than with a fixed g varying δ. We believe that careful measurements with proper setting conditions may approach a unique equilibrated value, which is the smallest value under various measuring conditions. However, many scattered values obtained experimentally tell insight of the micrometer-order inner structures.

F. Temperature dependence

Δ-dependent $D_{apparent}$ values approached an equilibrated value at longer Δ and larger g as shown in Figs. 4 and 5, respectively. In this situation, we observed the temperature-dependent diffusion at Δ = 70 ms at a fixed g of 9.8 T m^{-1}. The diffusion plots on the fixed measurement conditions are shown between 70 and 120 °C in Fig. 6.

Arrhenius plots for the $D_{apparent}$ values obtained at Δ = 70 ms and g = 9.8 T m^{-1} are shown in Fig. 7(a) and the values were slightly larger in the membrane sample than in the powder sample at every temperature. The activation energies were almost the same (33.3 ± 0.7 and 32.2 ± 1.4 kJ mol^{-1}) for the membrane and powder samples, respectively. These

RIGHTSLINK

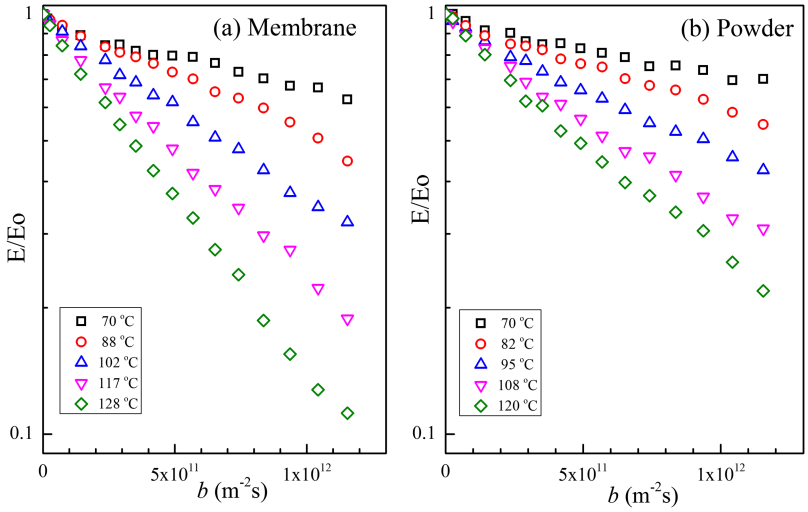

FIG. 6. Temperature-dependent diffusion plots for (a) the membrane and (b) powder samples measured at Δ = 70 ms and $g = 9.8$ T m^{-1}. The echo attenuation was obtained by varying δ = 0.2 to 4 ms. The $D_{apparent}$ values were 3.5, 6.4, 9.9, 14, and 19 × 10^{-13} m^2 s^{-1} at 70, 88, 102, 117, and 128 °C for the membrane sample, respectively. They were 3.1, 4.9, 7.2, 10, and 13 × 10^{-13} m^2 s^{-1} at 70, 82, 95, 108, and 120 °C, respectively, for the powder sample.

values were about three times larger than the activation energies of ^{7}Li T_1 in the same temperature range (10.2 ± 0.1 and 10.6 ± 0.1, for the membrane and powder samples, respectively), but about half that of the ionic conductivity. About one year later, we re-measured the $D_{apparent}$ at 120 °C for the samples. The absolute values were slightly smaller for both LLZO samples, although the trend of Δ-dependence was unchanged.

The temperature-dependent mean square displacement (MSD) $\sqrt{2D_{apparent}\Delta}$ in the μm space is shown in Fig. 7(b), in which the diffusion distance was slightly larger in the membrane sample and increased as the temperature increased in the micrometer space.

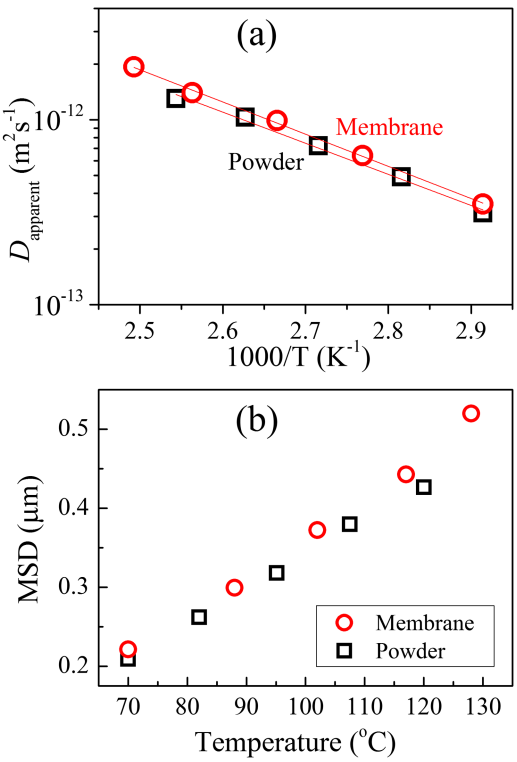

FIG. 7. (a) Arrhenius plots of $D_{apparent}$ values observed with $g = 9.8$ T m^{-1} and Δ = 70 ms, and (b) MSD plotted versus temperature for the membrane (circle) and powder (square) samples.

G. Diffractive patterns for short Δ

When Δ became short, the diffusion plots showed diffractive patterns in the present samples, as shown in Figs. 2 and 3. The Fourier-transformed (FT) echo attenuations show phase changes near minimum positions in a diffusive diffraction plot for electrolytes. Experimentally, the spectral phase changes are commonly encountered, but we cannot explain the phenomena theoretically for collisions between charged particles and environments. Then we always plot the magnitude-mode FT spectra of echo attenuations in Eq. (1) because the real-mode FT spectra pass through negative values. We confirm that if a plot were linear, the plots in real- or magnitude-mode data are not much different.

As reported previously, the diffractive patterns were insensitive to temperature, and in this study the LLZO was also insensitive to temperature. Here, we showed the diffractive patterns at 72 °C for four different Δ values from 5 to 20 ms, which are shown in q-space plots in Fig. 8(a) membrane and Fig. 8(b) powder samples. About one year later, we found that the diffracted patterns were reduced, as shown in Figs. 8(c) and 8(d). The reciprocals of q at the first diffusion minimum in the membrane sample were 4.2, 2.8, 2.1, and 1.8 μm for Δ = 5, 10, 15, and 20 ms, respectively, at the first measurements. For the later measurements, they were reduced to 3.0 and 2.1 μm for Δ = 5 and 10 ms, and no diffraction was observed for the longer Δ. Similarly, the diffraction distances of the powder sample were 3.8, 2.6, 2.0, and 1.6 μm for Δ = 5, 10, 15, and 20 ms, respectively, at the initial measurements and reduced to 2.7 and 1.8 μm for Δ = 5 and 10 ms, respectively, after one year. This phenomenon is probably related to decrease of the line width of the broad component of ^{7}Li spectra described above which contribute reduction of the collision.

The diffractive patterns are related to the inner and surface structures in the μm space. By the PGSE-NMR method, the diffusing procedures cannot be observed during the interval of the two PFGs. In a short time scale of less than 20 ms, we clearly observed the collision and diffraction for traveling lithium ions on walls composed of stationary lithium and anion species in the solid cubic LLZO. For longer Δ, the diffusive diffraction patterns were not observed due to averaging processes

RIGHTSLINK

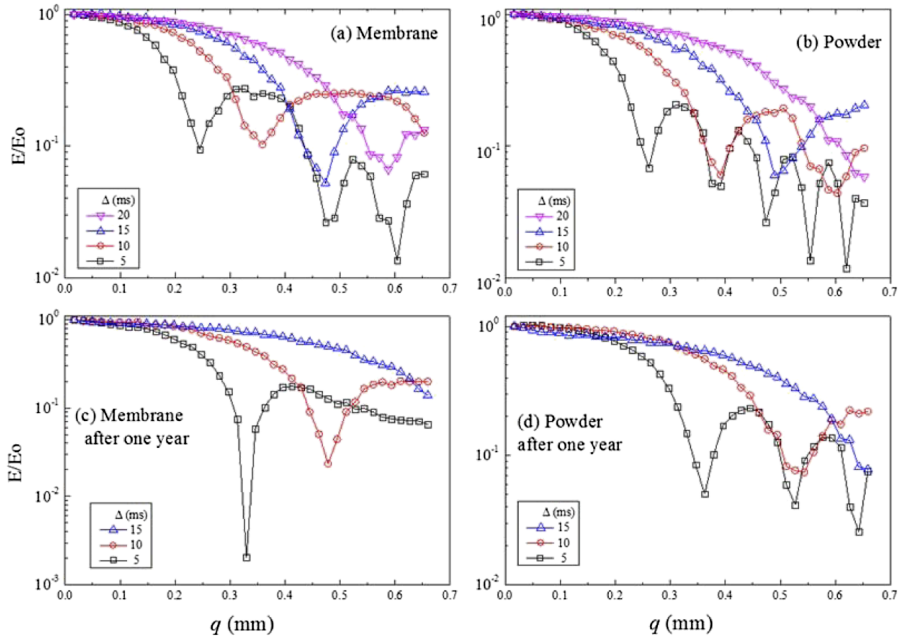

FIG. 8. Echo attenuation plots in q-space for (a) the membrane and (b) the powder samples for $\Delta = 5$, 10, 15, and 20 ms at a fixed $g = 9.8$ T m^{-1} with varying δ up to 4 ms. The plot profiles are observed at 72 °C. About one year later, the same measurements were performed for the flame-sealed samples for (c) the membrane and (d) powder samples.

including collision and diffraction. After one year, the diffraction patterns were reduced and the experimental results suggest that the lithium pathways in μm space became smoother to decrease the collisions owing to the structure relaxation in rigid parts of the solid conductors.

The MSD in Fig. 7 showed temperature dependence and the values were about 0.2 to 0.5 μm during 70 ms. At Δ = 10 ms, the estimated MSD value was about 0.7 μm and decreased with longer Δ (till 50 ms) and increased a little at Δ = 70 ms. The averaged traveling distances were much smaller than the diffraction distances. Then, within a short period, positive lithium ions migrate spontaneously in negatively charged circumstances on diffractive manners without thermal activation in the present temperature range. The diffractive migration may contribute little to the measured value of ionic conductivity.

H. One-dimensional ^{7}Li profile of the membrane sample

Using the pulse sequence in Fig. 1(b), temperature-dependent one-dimensional profiles were observed for the cubic-LLZO disk (diameter 3 mm and thickness 0.5 mm) in the direction of the thickness (z-gradient direction). The temperature was between 51 and 111 °C as shown in Fig. 9.

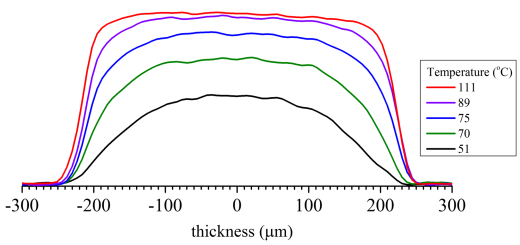

FIG. 9. One-dimensional profiles for a membrane disk (thickness = 0.5 mm) in the temperature between 51 and 111 °C. The τ value was set to 2.1 ms. One pixel was 7 μm. The measuring parameters were kept constant except for the repetition time, for fully recovered signals (five times T_1).

The area intensity of the one-dimensional profiles increased as the temperature increased, which must be related to the number of mobile lithium ions giving the ^{7}Li echo signals (τ = 2.1 ms). The area intensity is plotted against temperature in Fig. 10. Mobile lithium ions can produce ^{7}Li echo signals and must be related closely to the number of charge-carrier ions in the solid conductors. It was necessary to confirm the influence of T_2 on the area intensity. The measurements of one-dimensional profiles were performed at a fixed temperature, 74 °C by varying the τ value as shown in Fig. S6 of the supplementary material. The shape of the profiles changed little, but the area intensity decreased with longer τ and the decay curve was analyzed with T_2. The area intensities shown in Fig. 9 were plotted versus temperature in Fig. 10 and the T_2 effect was estimated. The temperature dependent echo intensities at (τ = 2.1 ms) were observed and plotted together in Fig. 10. Clearly, the area intensities are influenced by T_2, but the plots were not parallel in the temperature range observed.

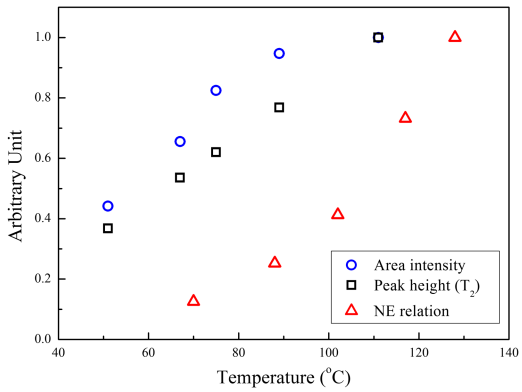

FIG. 10. Temperature dependence of the area intensity of one-dimensional plots for the membrane disk of the cubic LLZO in Fig. 9, the echo signal height at τ = 2.1 ms, and the ratio of numbers for lithium carrier ions calculated using the NE relation of Eq. (2).

RIGHTSLINK

Since anions do not contribute to ionic conductivity, the Nernst-Einstein relation can be simplified to[67]

$$D(T) = \frac{kT}{Ne^2}\sigma(T), \quad (2)$$

where e is the electron charge, and k is the Boltzmann's constant. In the present situation, N is the number of mobile lithium ions that contribute to the ionic conductivity, i.e., the number of charge-carrier ions at a given temperature. Using the ionic conductivity in Fig. S2 of the supplementary material and the values of D_{apparent} in Fig. 6, the temperature dependent carrier ion number N in Eq. (2) was estimated at each temperature and plotted in Fig. 10 together with the area intensity in Fig. 9 and peak height of echo signals at τ = 2.1 ms. The number of the carrier ions increased with temperature together with the area intensity and peak height of the echo signal.

In addition to the increase of area intensity with the increased temperature, the number of lithium ions in the surface area increased. This specific pattern suggests that thermal activation is necessary for mobile lithium ions to approach the surface area. This feature is quite different in the lithium profiles in polymer electrolytes, in which the surface area was always filled by ^{7}Li profile at any temperature.[68] Thermal expansion has been reported as an evolution of the lattice constant during the heating step for LLZO (0.3 wt. % Al) studied by XRD.[69] The increased of presence of mobile lithium ions in the surface area may relate to the thermal expansion. It was reported that the surface microstructure influences the cycle performance.[70] The one-dimensional profiles for the presence of lithium ions near the surface will give information on the surface morphology.

IV. CONCLUSION

A garnet-type cubic LLZO was studied in membrane and powder samples using ^{7}Li NMR spectroscopy to observe lithium ion migration in μm (10^{-6} m) space. The PGSE-NMR method can vary the observation time length, in which the lithium ions diffuse more quickly in shorter time intervals and collide with the stationary anions and immobile lithium ions and are diffracted in short time intervals. The lithium ions in the membrane sample can travel slightly longer distances before collision than in the powder sample. For the longer observation time in ms order, the lithium ions gradually lose speed in migration owing to averaging processes including collisions and diffractions and approach an equilibrated value ($D_{\text{equilibrated}}$, close to tracer diffusion constant). The membrane sample had slightly larger values of D_{apparent} than with the powder samples while the activation energies were almost the same at 33 and 32 kJ mol^{-1} for the membrane and powder samples, respectively. The lithium ion diffusion phenomena depend on the PFG strength, suggesting that the lithium ion migration distributes widely in μm space with heterogeneous and polydispersive manners. The time and PFG depending lithium ion diffusion was also observed in LLZO-Ta and sulfide-type solid conductors, and lithium ion migration in μm space showed common features.

One-dimensional profiles indicated that the area intensity increased with increased temperature under influences of elongated T_2. Interestingly, the population near the surface area also increased as the temperature increased. The increase in the number of charge-carrier ions was estimated using the Nernst-Einstein relation from the ionic conductivity and the lithium equilibrated D_{apparent} value close to the tracer diffusion constant in the μm space. The feature resembled the increase of the area intensity of the one-dimensional profiles in which migrating lithium ions have long T_2 values.

SUPPLEMENTARY MATERIAL

See supplementary material for the additional figures of SEM images, ionic conductivity, ^{7}Li spectrum at 80 °C, temperature dependences of the ^{7}Li line widths for narrow and broad components, ^{7}Li T_1 and T_2, and one-dimensional profiles depending on τ at 74 °C (supplementary material 1) and good rectangular PFG shapes of our hardware, calibration of g and δ, negligible background DC current effect, and the PGSE NMR measurements for short T_2 (supplementary material 2).

ACKNOWLEDGMENTS

K.H. wishes to thank Professor K. Kose (University of Tsukuba, Japan) for helpful discussion while performing the research.

[1] V. Thangadurai, S. Narayanan, and D. Pinzaru, Chem. Soc. Rev. **43**, 4714 (2014).
[2] R. Murugan, V. Thangadurai, and W. Weppner, Angew. Chem., Int. Ed. **46**, 7778 (2007).
[3] J. Awaka, N. Kijima, H. Hayakawa, and J. Akimoto, J. Solid State Chem. **182**, 2046 (2009).
[4] E. J. Cussen, J. Mater. Chem. **20**, 5167 (2010).
[5] J. Awaka, A. Takashima, K. Kataoka, N. Kijima, Y. Idemoto, and J. Akimoto, Chem. Lett. **40**, 60 (2011).
[6] S. Toda, K. Ishiguro, Y. Shimonishi, A. Hirano, Y. Takeda, O. Yamamoto, and N. Imanishi, Solid State Ionics **233**, 102 (2013).
[7] C. Galven, J.-L. Fourquet, M.-P. Crosnier-Lopez, and F. Berre, Chem. Mater. **23**, 1892 (2011).
[8] G. Larraz, G. A. Orera, and M. L. Sanjuán, J. Mater. Chem. A **1**, 11419 (2013).
[9] G. Larraz, A. Orera, J. Sanz, I. Sobrados, V. Diez-Gómez, and M. L. Sanjuán, J. Mater. Chem. A **3**, 5683 (2015).
[10] C. A. Geiger, E. Alekseev, B. Lazic, M. Fisch, T. Armbruster, R. Langner, M. Fechtelkord, N. Kim, T. Pettke, and W. Weppner, Inorg. Chem. **50**, 1089 (2011).
[11] A. Düvel, A. Kuhn, L. Robben, M. Wilkening, and P. Heitjans, J. Phys. Chem. C **116**, 15192 (2012).
[12] S. Ohta, T. Kobayashi, and T. Asaoka, J. Power Sources **196**, 3342 (2011).
[13] Y. Wang and W. Lai, Electrochem. Solid-State Lett. **15**, A68 (2012).
[14] S. Narayanan, F. Ramezanipour, and V. Thangadurai, J. Phys. Chem. C **116**, 20154 (2012).
[15] S. Ramakumar, L. Satyanarayana, S. V. Manorama, and R. Murugan, Phys. Chem. Chem. Phys. **15**, 11327 (2013).
[16] T. Thompson, J. Wolfenstine, J. L. Allen, M. Johannes, A. Huq, I. N. David, and J. Sakamoto, J. Mater. Chem. A **2**, 13431 (2014).
[17] S. Ramakumar, N. Janani, and R. Murugan, Dalton Trans. **44**, 539 (2015).
[18] H. Zhang, X. Liu, Y. Qi, and V. Liu, J. Alloys Compd. **577**, 57 (2013).
[19] Y. Suzuki, K. Kami, K. Watanabe, A. Watanabe, N. Saito, K. Ohnishi, A. Takada, R. Sudo, and N. Imanishi, Solid State Ionics **278**, 172 (2015).
[20] S. Mukhopadhyay, T. Thompson, J. Sakamoto, A. Huq, J. Wolfenstine, J. Allen, L. Jan, N. Bernstein, D. A. Stewart, and M. D. Johannes, Chem. Mater. **27**, 3658 (2015).
[21] Y. Chen, E. Rangasamy, C. Liang, and K. An, Chem. Mater. **27**, 5491 (2015).
[22] M. M. Ahmad and A. Al-Jaafari, J. Mater. Sci.: Mater. Electron. **26**, 8136 (2015).
[23] Y. Matsuda, Y. Itami, K. Hayamizu, T. Ishigami, M. Matsui, Y. Takeda, O. Yamamoto, and N. Imanishi, RSC Adv. **6**, 78210 (2016).

RIGHTSLINK

[24]T. Yang, Z. D. Gordon, Y. Li, and C. K. Chan, J. Phys. Chem. C **119**, 14947 (2015).
[25]R. P. Rao, W. Gu, N. Sharma, V. K. Peterson, M. Avdeev, and S. Adams, Chem. Mater. **27**, 2903 (2015).
[26]N. Bernstein, M. D. Johannes, and K. Hoang, Phys. Rev. Lett. **109**, 205702 (2012).
[27]R. Jalem, Y. Yamamoto, H. Shiiba, M. Nakayama, H. Munakata, T. Kasuga, and K. Kanamura, Chem. Mater. **25**, 425 (2013).
[28]M. Klenk and W. Lai, Phys. Chem. Chem. Phys. **17**, 8758 (2015).
[29]D. Wang, G. Zhong, W. K. Pang, Z. Guo, Y. Li, M. J. McDonald, R. Fu, J.-X. Mi, and Y. Yang, Chem. Mater. **27**, 6650 (2015).
[30]M. Matsui, K. Takahashi, K. Sakamoto, A. Hirano, Y. Takeda, O. Yamamoto, and N. Imanishi, Dalton Trans. **43**, 1019 (2014).
[31]M. Matsui, K. Sakamoto, K. Takahashi, A. Hirano, Y. Takeda, O. Yamamoto, and N. Imanishi, Solid State Ionics **262**, 155 (2014).
[32]Y. Matsuda, K. Sakamoto, M. Matsui, O. Yamamoto, Y. Takeda, and N. Imanishi, Solid State Ionics **277**, 23 (2015).
[33]J. Han, J. Zhu, Y. Li, X. Yu, S. Wang, G. Wu, H. Xie, S. C. Vogel, F. Izumi, K. Momma, Y. Kawamura, J. B. Goodenough, and Y. Zhao, Chem. Commun. **48**, 9840 (2012).
[34]H. Xie, J. A. Alonso, Y. Li, M. T. Fernández-Díaz, and J. B. Goodenough, Chem. Mater. **23**, 3587 (2011).
[35]M. Xu, M. S. Park, J. M. Lee, T. Y. Kim, Y. S. Park, and E. Ma, Phys. Rev. B **85**, 052301 (2012).
[36]R. Jalem, M. Nakayama, W. Manalastas, Jr., J. A. Kilner, R. W. Grimes, T. Kasuga, and K. Kanamura, J. Phys. Chem. C **119**, 20783 (2015).
[37]Y. Wang, M. Klenk, K. Page, and W. Lai, Chem. Mater. **26**, 5613 (2014).
[38]M. P. O'Callaghan, A. S. Powell, J. J. Titman, G. Z. Chen, and E. J. Cussen, Chem. Mater. **20**, 2360 (2008).
[39]M. M. Ahmad, RSC Adv. **5**, 25824 (2015).
[40]M. M. Ahmad, Nanoscale Res. Lett. **10**, 58 (2015).
[41]D. Rettenwander, J. Langer, W. Schmidt, C. Arrer, K. J. Harris, V. Terskikh, G. R. Goward, M. Wilkening, and G. Amthauer, Chem. Mater. **27**, 3135 (2015).
[42]H. Buschmann, J. Dölle, S. Berendts, A. Kuhn, P. Bottke, M. Wilkening, P. Heitjans, A. Senyshyn, H. Ehrenberg, A. Lotnyk, V. Duppel, L. Kienle, and J. Janek, Phys. Chem. Chem. Phys. **13**, 19378 (2011).
[43]A. Kuhn, S. Narayanan, L. Spencer, G. Goward, V. Thangadurai, and M. Wilkening, Phys. Rev. B **83**, 094302 (2011).
[44]B. Koch and M. Vogel, Solid State Nucl. Magn. Reson. **34**, 37 (2008).
[45]A. Kuhn, V. Epp, G. Schmidt, S. Narayanan, V. Thangadurai, and M. Wilkening, J. Phys.: Condens. Matter **24**, 035901 (2012).
[46]P. Bottke, D. Rettenwander, W. Schmidt, G. Amthauer, and M. Wilkening, Chem. Mater. **27**, 6571 (2015).
[47]A. Kuhn, M. Kunze, P. Sreeraj, H.-D. Wiemhöfer, V. Thangadurai, M. Wilkening, and P. Heitjans, Solid State Nucl. Magn. Reson. **42**, 2 (2012).
[48]K. Hayamizu, Y. Aihara, S. Arai, and C. Garcia-Martinez, J. Phys. Chem. B **103**, 519 (1999).
[49]Y. Aihara, K. Sugimoto, W. S. Price, and K. Hayamizu, J. Chem. Phys. **113**, 1981 (2000).
[50]K. Hayamizu, J. Chem. Eng. Data **57**, 2012 (2012).
[51]K. Hayamizu, Y. Aihara, and W. S. Price, J. Chem. Phys. **113**, 4785 (2000).
[52]K. Hayamizu, K. Sugimoto, E. Akiba, Y. Aihara, T. Bando, and W. S. Price, J. Phys. Chem. B **106**, 547 (2002).
[53]K. Hayamizu, Y. Matsuda, M. Matsui, and N. Imanishi, Solid State Nucl. Magn. Reson. **70**, 21 (2015).
[54]K. Hayamizu and Y. Aihara, Solid State Ionics **238**, 7 (2013).
[55]K. Hayamizu, Y. Aihara, and N. Machida, Solid State Ionics **259**, 59 (2014).
[56]K. Hayamizu, Y. Aihara, T. Watanabe, T. Yamada, S. Ito, and N. Machida, Solid State Ionics **285**, 51 (2016).
[57]P. T. Callaghan, K. W. Jolley, and J. Leliever, Biophys. J. **28**, 133 (1979).
[58]P. T. Callaghan, A. Coy, D. MacGowan, K. J. Packer, and F. O. Zelaya, Nature **351**, 467 (1991).
[59]A. Caprihan, L. Z. Wang, and E. Fukushima, J. Magn. Reson., Ser. A **118**, 94 (1996).
[60]S. L. Codd and P. T. Callaghan, J. Magn. Reson. **137**, 358 (1999).
[61]W. S. Price, *NMR Studies of Translational Motion* (Cambridge University Press, New York, 2009).
[62]P. T. Callaghan, *Translational Dynamics and Magnetic Resonance* (Oxford University Press, Oxford, 2011).
[63]J. Kärger and R. Valiullin, Chem. Soc. Rev. **42**, 4172 (2013).
[64]K. Hayamizu, S. Tsuzuki, S. Seki, and Y. Umebayashi, J. Chem. Phys. **135**, 084505 (2011).
[65]E. O. Stejskal and J. E. Tanner, J. Chem. Phys. **42**, 288 (1965).
[66]J. E. Tanner, J. Chem. Phys. **52**, 2523 (1970).
[67]C. Julien and G.-A. Nazri, *Solid State Batteries: Material Design and Optimization* (Kluwer Academic Publishers, Boston, 1994).
[68]S. Seki, T. Kobayashi, K. Takai, K. Hayamizu, and M. Watanabe, oral presentation in 41st Symposium on Solid State Ionics of Japan, Sapporo, Japan, 27 November 2015.
[69]A. A. Hubaud, D. J. Schroeder, B. J. Ingram, J. S. Okasinski, and J. T. Vaughey, J. Alloys Compd. **644**, 804 (2015).
[70]L. Cheng, W. Chen, M. Kunz, K. Persson, N. Tamura, G. Chen, and M. Doeff, ACS Appl. Mater. Interfaces **7**, 2073 (2015).

RIGHTSLINK